Evaluation of local electric fields generated by transcranial direct current stimulation with an extracephalic reference electrode based on realistic 3D body modeling

2012 Phys. Med. Biol. 57 2137

(http://iopscience.iop.org/0031-9155/57/8/2137)

IOP Publishing Physics in Medicine and Biology

Phys. Med. Biol. **57** (2012) 2137–2150 doi:10.1088/0031-9155/57/8/2137

Evaluation of local electric fields generated by transcranial direct current stimulation with an extracephalic reference electrode based on realistic 3D body modeling

Chang-Hwan Im[1,3], **Ji-Hye Park**[1], **Miseon Shim**[1], **Won Hyuk Chang**[2] **and Yun-Hee Kim**[2]

[1] Department of Biomedical Engineering, Hanyang University, Seoul, Korea
[2] Department of Physical and Rehabilitation Medicine, Samsung Medical Center, Sungkyunkwan University School of Medicine, Seoul, Korea

E-mail: ich@hanyang.ac.kr

Received 13 August 2011, in final form 25 January 2012
Published 28 March 2012
Online at stacks.iop.org/PMB/57/2137

Abstract

In this study, local electric field distributions generated by transcranial direct current stimulation (tDCS) with an extracephalic reference electrode were evaluated to address extracephalic tDCS safety issues. To this aim, we generated a numerical model of an adult male human upper body and applied the 3D finite element method to electric current conduction analysis. In our simulations, the active electrode was placed over the left primary motor cortex (M1) and the reference electrode was placed at six different locations: over the right temporal lobe, on the right supraorbital region, on the right deltoid, on the left deltoid, under the chin, and on the right buccinator muscle. The maximum current density and electric field intensity values in the brainstem generated by the extracephalic reference electrodes were comparable to, or even less than, those generated by the cephalic reference electrodes. These results suggest that extracephalic reference electrodes do not lead to unwanted modulation of the brainstem cardio-respiratory and autonomic centers, as indicated by recent experimental studies. The volume energy density was concentrated at the neck area by the use of deltoid reference electrodes, but was still smaller than that around the active electrode locations. In addition, the distributions of elicited cortical electric fields demonstrated that the use of extracephalic reference electrodes might allow for the robust prediction of cortical modulations with little dependence on the reference electrode locations.

(Some figures may appear in colour only in the online journal)

[3] Author to whom any correspondence should be addressed.

1. Introduction

Transcranial direct current stimulation (tDCS) is a noninvasive brain electrical stimulation technique that can modulate cortical excitability by transmitting a small direct current between a pair of scalp electrode pads (Antal *et al* 2004, Fregni *et al* 2005, Nitsche and Paulus 2000, Nitsche *et al* 2007, 2008, Wagner *et al* 2007b, Williams *et al* 2009). The tDCS technique has been studied in a variety of clinical fields, especially as a potential treatment tool for neuropsychiatric diseases and neurological disorders including depression, epilepsy, electroanalgesia, stroke, Alzheimer's disease, chronic pain, tinnitus, and Parkinson's disease (Nitsche *et al* 2009, Fregni *et al* 2006, 2007, Mignon *et al* 1996, Boggio *et al* 2007, Ferrucci *et al* 2008, Fregni and Pascual-Leone 2007, Schlaug *et al* 2008, Williams *et al* 2009). Although the effect of tDCS treatment is similar to that of repetitive transcranial magnetic stimulation (rTMS) and is less focal than that of rTMS, tDCS has attracted great attention in neuroscience as it has several advantages over traditional rTMS treatment including ease of implementation, better mobility, good safety profile, and lower cost (Nitsche *et al* 2008, Priori 2003, Williams *et al* 2009).

Traditionally, tDCS systems use anode and cathode electrodes at empirically determined locations considering the targeted brain area. Extensive clinical studies have shown that anodal and cathodal tDCS facilitate and inhibit cortical excitability, respectively, although the exact underlying mechanisms have not yet been revealed (Antal *et al* 2001, Kincses *et al* 2004, Nitsche *et al* 2008). The most widely used electrode montage is the so-called 'bi-cephalic' electrode montage where both of the two electrode pads are attached to specific locations on the scalp surface, e.g. the 'active' electrode on M1 and the 'reference' electrode on the opposite hemisphere (Nitsche and Paulus 2000). One of the limitations of this electrode montage is that it is difficult to exclude the effect of the reference electrode since the observed tDCS effects could be due to a combination of the modulations of both active and reference electrodes (Nitsche *et al* 2007). Moreover, it is generally accepted that for a fixed active electrode position, varying the location of the reference electrode can influence the current distribution formed inside the brain and thereby affect the resultant brain activity modulation (Cogiamanian *et al* 2007, Nitsche and Paulus 2000, Mendonca *et al* 2011, Priori *et al* 2008). The simplest way to address this issue is to use an extracephalic reference electrode montage that places the reference electrode outside the scalp area (Accornero *et al* 2007, Galea *et al* 2009, Koenigs *et al* 2009, Monti *et al* 2008, Priori *et al* 2008, Vandermeeren *et al* 2010, Fertonani *et al* 2010, Cogiamanian *et al* 2007, Ferrucci *et al* 2008, Moliadze *et al* 2010, Mahmoud *et al* 2010)[4]. Nevertheless, the use of an extracephalic reference electrode has been often avoided since the earliest tDCS studies conducted by Lippold and collaborators (Lippold and Redfearn 1964, Redfearn *et al* 1964) warned that the use of an extracephalic reference electrode could lead to an unwanted modulation of the brainstem cardio-respiratory and autonomic centers.

Although classical bi-cephalic electrode montages are most often used, some recent studies have reported the successful application of tDCS with an extracephalic reference electrode without any notable changes in heart rate, blood pressure, body temperature, or respiratory frequency (Accornero *et al* 2007, Galea *et al* 2009, Koenigs *et al* 2009, Monti *et al* 2008, Vandermeeren *et al* 2010). These experimental studies facilitated the development of a series of experimental conditions in which tDCS with an extracephalic reference electrode could be applied safely. For example, Vandermeeren *et al* (2010) confirmed that a 20 min dc stimulation with an active electrode on the midline Fz and a reference electrode over the right tibia did not

[4] Throughout the entire manuscript, the reference electrode attached on the scalp surface will be referred to as 'cephalic reference electrode', while that attached outside the scalp area will be referred to as 'extracephalic reference electrode' (Moliadze *et al* 2010).

provoke any changes in the vital parameters of healthy subjects. Despite these experimental studies, however, it is still unexplored how much amount of current is actually passing through the brainstem and other sub-cortical nuclei when an extracephalic reference electrode is used relative to a cephalic reference electrode.

Since no imaging modality is currently able to image the electric field distribution generated by tDCS during *in vivo* human experiments, the electric field distributions are estimated from numerical field simulations using realistic head models derived from structural magnetic resonance (MR) imaging (Miranda *et al* 2006, Wagner *et al* 2007a, Datta *et al* 2009, 2010, Im *et al* 2008, Park *et al* 2011). Indeed, 3D field simulations based on the 3D finite element method (FEM) widened our insights into the underlying mechanisms of stimulating current conduction (Dmochowski *et al* 2011, Miranda *et al* 2006, 2007, Wagner *et al* 2007a, Datta *et al* 2010, Holdefer *et al* 2006), accelerated the development of new electrode montages (Datta *et al* 2009, Dmochowski *et al* 2011, Im *et al* 2008, Park *et al* 2011), and enabled more accurate field concentrations to targeted brain areas (Dmochowski *et al* 2011, Halko *et al* 2011, Mendonca *et al* 2011). In this study, we adopted the 3D FEM for the numerical computation of electric fields generated by tDCS inside a simulated human body. We generated a numerical model of an adult human male upper body with a reasonable resolution and evaluated electric field intensity and current density values at the brainstem and other sub-cortical nuclei with respect to different electrode montages including extracephalic references.

2. Methods and materials

2.1. 3D FEM

The 3D FEM was adopted to analyze the current density distribution inside the human body produced by tDCS. Considering direct current conduction, the following electrostatic Laplace equation was used as the governing equation of the FEM:

$$\nabla \cdot (\sigma \nabla V) = 0, \tag{1}$$

where σ and V represent the electrical conductivity and electric potential, respectively. We used a first-order finite element (FE) formulation and incomplete Cholesky conjugate gradient (ICCG) matrix solver (Jin 2002). The convergence criterion of ICCG was $|\mathbf{A}\boldsymbol{x} - \mathbf{b}|/|\mathbf{b}| < 1.0 \times 10^{-14}$, where $\mathbf{A}$, $\boldsymbol{x}$, and $\mathbf{b}$ represent a stiffness matrix, unknown vector, and forcing vector, respectively. Two electrode pads were modeled as two sets of surface nodes, each with different Dirichlet-type boundary values, e.g. -1 and 1 V, respectively. The current density was evaluated for every volumetric tetrahedral element using the solution of (1) and then transformed into a node-wise form by interpolation. The total injection current value was computed by integrating the total current density under each surface electrode pad area. The average difference between the total injection currents of two electrodes was less than 6% of the absolute injection current value in our simulations (5.89% $\pm$ 1.74%). Based on the linearity between the total injection current and the current density at each node, the current density vectors in the entire analysis domain were scaled by a ratio of the target injection current (1 mA in this study) to the computed total injection current, which consequently led to a result for a constant current injection through a pair of electrode pads (injection current of each pad: 1 and –1 mA, respectively). All numerical analyses were performed using an optimized in-house FEM program coded using Fortran 90 (Im *et al* 2008).

2.2. 3D realistic modeling of an adult male human upper body

For the accurate evaluation of conductive current flow inside a human body, a reasonable resolution model of an adult male upper body was generated from a whole-body CAD model, originating from the Virtual Family project (Christ *et al* 2010). We used a 1 mm resolution volume pixel (voxel) dataset consisting of more than 80 pre-classified tissue types acquired from whole-body MR images of a healthy European 34 year old male (referred to as *Duke*), whose height, weight, and BMI were 1.74 m, 70.0 kg, and 23.1 kg m^{-2}, respectively.

To generate the FE model from the voxel dataset, we first separately extracted voxels included in the 15 different tissue types, which were skin, skull, brain, larynx, pharynx, left lung, right lung, spinal cord, thalamus, hippocampus, cerebellum, midbrain, pons, medulla, and spinal cord. Then, each structure surface was tessellated with surface triangular elements, forming closed surface mesh structures. We used a free software package (MeshLab; http://meshlab.sourceforge.net) to generate surface meshes (Cignoni *et al* 2008). The initial mesh structures shown in figure 1 (left figure) was generated from the point cloud data of each tissue using the ball-pivoting algorithm (BPA) (Bernardini *et al* 1999), which forms triangles by repeatedly pivoting a ball around an edge until it touches another point. The BPA variables, such as pivoting ball radius, clustering radius, and angle threshold, were determined independently for each mesh structure after an extensive trial-and-error process. Since the initial mesh structure was generally noisy, it was smoothed using an extended version of Laplacian smoothing (Vollmer *et al* 1999). Since the extensive geometrical smoothing could eliminate details such as strong curvatures in some structures and thereby affect the solution accuracy, we adjusted the level of smoothing by carefully inspecting the geometrical shape deformation. After removing duplicated points, duplicated surfaces, isolated surfaces, and zero-area elements, the closed surface mesh structure of each tissue was constructed (figure 1, left figure). Then, the independently modeled mesh structures were integrated into a single upper body model as shown in figure 1. The integrated model was tessellated with volumetric tetrahedral elements using an open-source mesh generation software package (TetGen; http://tetgen.belios.de), which was based on the constrained Delaunay tetrahedralization approach (Si 2008). No meshes were generated inside the left lung, right lung, larynx, and pharynx because these structures conduct negligible electric current. The minimum radius–edge ratio was set to 1.8 to generate high quality tetrahedral elements, and the maximum volume of each tetrahedron was set to 50 mm^3. The tetrahedralized upper body model consisted of 98 119 nodes and 590 104 elements. The average volume of the generated tetrahedral elements was 20.1 $\pm$ 12.9 mm^3, corresponding to a 2.7 mm $\times$ 2.7 mm $\times$ 2.7 mm size voxel. In some complicated structures, relatively smaller elements were generated by controlling the size of initial surface meshes. For example, the average volume of tetrahedral elements in spinal cord was 6.15 $\pm$ 3.55 mm^3, that of thalamus was 9.22 $\pm$ 5.34 mm^3, and that of hippocampus was 12.2 $\pm$ 7.51 mm^3. We then assigned regional attributes for internal air, vertebrae, bone, and fat (which were difficult to generate in closed surface mesh structures) to proper tetrahedral elements in the tessellated body model (see figure 1, right figures) when the minimum distance between each tetrahedral element and adjacent point cloud of the four structures was less than 3 mm. Muscle was not modeled independently since its electrical conductivity value was not significantly different from that of skin (Gabriel *et al* 1996a, 1996b, Sadleir *et al* 2010).

Figure 1(a) shows the final upper body model, with the mesh structures other than the brain and nervous system shown in a central figure and those of the brain and nervous systems in a left figure. Figure 1(b) shows the cross-sectional cuts of the volume meshes to demonstrate the level of detail of our body model. The electrical conductivity profiles for each

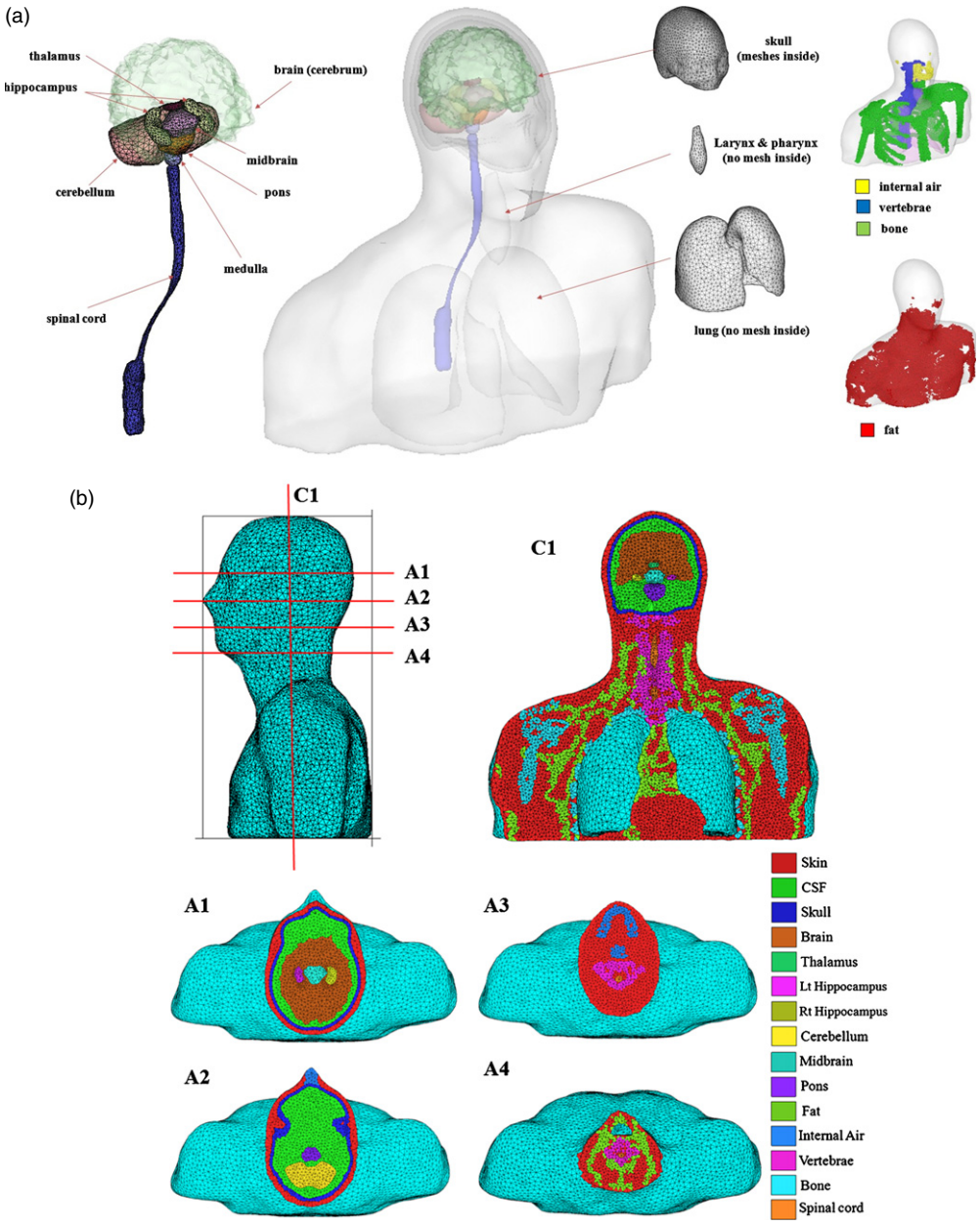

Figure 1. (a) The FE model of the adult male upper body: (left figure) mesh structures of the brain and nervous system; (middle figure) mesh structures other than the brain and nervous system. Meshes were not generated inside the left lung, right lung, larynx, and pharynx; (right figures) assigned regional attributes of four complex structures (internal air, vertebrae, bone, and fat). Each dot represents a tetrahedral element. (b) Cross-sectional cuts of the volume meshes: four axial cuts (A1–A4) and one coronal cut (C1) are visualized, where different tissue types are coded in color. The positions of the cut planes are illustrated in the upper left figure.

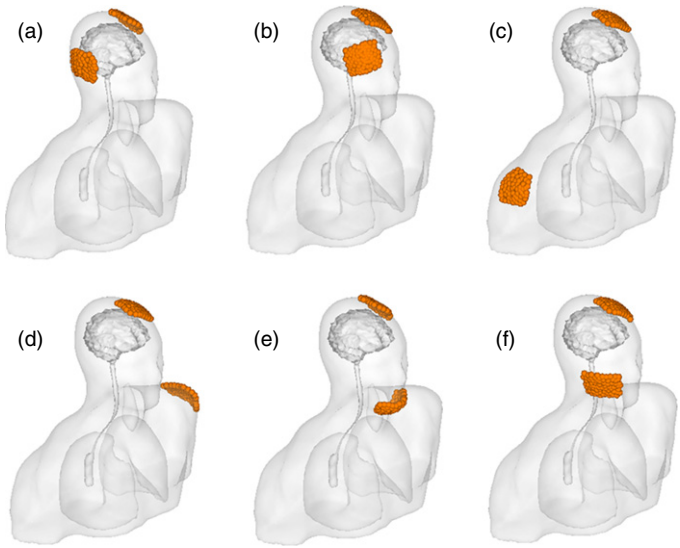

Figure 2. Locations of active and reference electrodes. Reference electrode locations: (a) over the right temporal lobe (Type A), (b) on the right supraorbital region (Type B), (c) on the right deltoid (Type C), (d) on the left deltoid (Type D), (e) under the chin (Type E), (f) on right buccinator muscle (Type F). Each set of clustered dots represents each electrode pad.

Table 1. Electrical conductivities assigned to tissues in the adult male upper body model. Conductivity values were chosen from low frequency (<1 kHz) data in the literature.

Tissue types	Conductivity (S m^{-1})	References
Skin	4.3×10^{-1}	Haueisen *et al* (1997), Sadleir *et al* (2010)
CSF	1.5×10^{0}	Haueisen *et al* (1997)
Bone (incl. vertebrae and skull)	1.5×10^{-2}	Oostendorp *et al* (2000)
Fat	2.5×10^{-2}	Gabriel *et al* (1996a, 1996b)
Brain (cerebrum)	2.0×10^{-1}	Mean of Haueisen *et al* (1997)
	2.0×10^{-1}	Gabriel *et al* (1996a)
Spinal cord and cerebellum	1.5×10^{-1}	Haueisen *et al* (1997)
Brainstem (medulla, pons, and midbrain)	4.7×10^{-1}	Gabriel *et al* (1996a, 1996b)
Hippocampus and thalamus	1.0×10^{0}	Holsheimer (1987), Gabriel *et al* (1996a, 1996b)

tissue were obtained from the literature (Haueisen *et al* 1997, Sadleir *et al* 2010, Oostendorp *et al* 2000, Gabriel *et al* 1996a, 1996b, Holsheimer 1987) and are summarized in table 1. The active electrode (anode) and reference electrode (cathode) were modeled as two rectangular pads (7×5 cm^2 each). Figure 2 shows the locations of the active and reference electrodes. The active electrode was attached over the left primary hand motor cortex (M1), while the reference electrode was placed at six different locations (figure 2), over the contralateral temporal lobe (Hummel *et al* 2010), on the contralateral supraorbital region (Datta *et al* 2009), on the right deltoid (Cogiamanian *et al* 2007), on the left deltoid, under the chin (Priori *et al* 1998), and on the right buccinator muscle (Galea *et al* 2009). Based on previous studies, either the contralateral shoulder, deltoid, or upper arm is most frequently

Table 2. Maximum electric field intensity (E, unit: V m^{-1}), current density (J, unit: A m^{-2}), and volume energy density (σE^2, unit: J m^{-3}) values at various brain tissues generated by six different electrode montages.

Tissue	Quantity	Type A	Type B	Type C	Type D	Type E	Type F
Skin	E	1.7499	2.6010	1.5665	1.8018	2.0719	2.1711
	J	0.7992	1.1509	0.7707	0.8407	0.8288	0.8684
	σE^2	1.31	2.76	1.02	1.12	1.80	1.94
Cerebral cortex	E	0.9970	0.9927	0.8852	0.9047	0.9309	0.8961
	J	0.0150	0.0149	0.0133	0.0136	0.0140	0.0134
	σE^2	1.50×10^{-2}	1.50×10^{-2}	1.18×10^{-2}	1.24×10^{-2}	1.3×10^{-2}	1.22×10^{-2}
Spinal cord	E	0.1612	0.0700	0.7534	0.7535	0.3824	0.1769
	J	0.1358	0.0612	0.2163	0.2096	0.1478	0.1441
	σE^2	2.05×10^{-2}	4.32×10^{-3}	0.12	0.11	2.41×10^{-2}	2.40×10^{-2}
Midbrain	E	0.4726	0.2431	0.4118	0.4255	0.5093	0.3864
	J	0.0071	0.0036	0.0062	0.0064	0.0076	0.0058
	σE^2	3.35×10^{-2}	8.89×10^{-4}	2.54×10^{-3}	2.72×10^{-3}	3.90×10^{-3}	2.24×10^{-3}
Pons	E	0.3776	0.1760	0.4361	0.4551	0.4684	0.3626
	J	0.0057	0.0026	0.0071	0.0073	0.0070	0.0054
	σE^2	2.14×10^{-3}	4.66×10^{-4}	4.48×10^{-3}	4.81×10^{-3}	3.29×10^{-3}	1.97×10^{-3}
Medulla	E	0.2355	0.1064	0.3361	0.3551	0.3496	0.3020
	J	0.1367	0.0621	0.0747	0.0676	0.1652	0.1470
	σE^2	1.89×10^{-2}	4.05×10^{-3}	2.94×10^{-3}	3.05×10^{-3}	2.77×10^{-2}	2.25×10^{-2}
Hippocampus	E	0.5638	0.2336	0.4271	0.4439	0.5544	0.4187
	J	0.0085	0.0035	0.0064	0.0067	0.0083	0.0063
	σE^2	4.79×10^{-3}	8.21×10^{-4}	2.74×10^{-3}	2.96×10^{-3}	4.61×10^{-3}	2.63×10^{-3}
Thalamus	E	0.5141	0.2974	0.4191	0.4310	0.4607	0.4129
	J	0.0077	0.0045	0.0063	0.0065	0.0069	0.0062
	σE^2	3.97×10^{-3}	1.33×10^{-3}	2.64×10^{-3}	2.79×10^{-3}	3.19×10^{-3}	256×10^{-3}

Type A: left M1–right temporal lobe; Type B: left M1–right supraorbital region; Type C: left M1–right deltoid; Type D: left M1–left deltoid; Type E: left M1–chin; Type F: left M1–right buccinator muscle.

selected when the extracephalic reference electrode was attached to the upper body of a subject (Monti *et al* 2008, Fertonani *et al* 2010, Priori *et al* 2008, Cogiamanian *et al* 2007, Koenigs *et al* 2009, Ferrucci *et al* 2008, Moliadze *et al* 2010, Mahmoud *et al* 2010). Attaching a reference electrode to the face (e.g. under the chin, on the inferior cheek, on the anterior neck) is not usual, but was occasionally done in a few experimental studies (Galea *et al* 2009, Priori *et al* 1998, Berryhill *et al* 2010, Accornero *et al* 2007). One of the popular extracephalic reference electrode locations was the contralateral leg, either at the tibia, thigh, or knee (Lippold and Redfearn 1964, Redfearn *et al* 1964, Vandermeeren *et al* 2010, Carney 1969, Arfai *et al* 1970), but we did not consider those locations in this study due to the significantly increased complexity in modeling and computation. For the six different electrode montages, the maximum current density and maximum electric field intensity values at the skin, cerebral cortex, spinal cord, midbrain, pons, medulla, hippocampus, and thalamus were evaluated.

3. Results

We first compared the maximum current density and maximum electric field intensity values from various brain tissues among the six different electrode montages (table 2). The examples of electric field distributions in the brainstem and the spinal cord are shown in figure 3. The

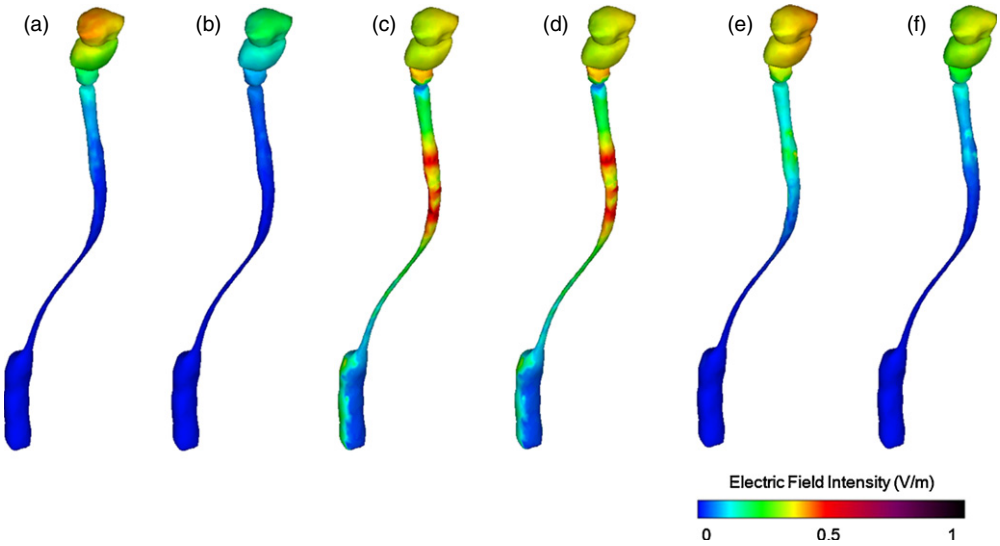

Figure 3. Distributions of electric fields in the brainstem and the spinal cord. Figure indices A–F represent different electrode configurations, respectively corresponding to Types A–F (please refer to the caption of figure 2).

maximum current density values in the brainstem (midbrain, pons, and medulla) generated by the reference electrodes on the right or left deltoid were not significantly different from, or was less than, those generated by the conventional cephalic reference electrodes (table 2). The maximum current densities of the other brain structures generated by the extracephalic reference on the right or left deltoid were also comparable to those of the cephalic references. The only distinct difference was observed at the spinal cord (table 2 and figure 3), where the maximum current density generated by tDCS with deltoid references was approximately twice that of the tDCS with cephalic references. Although twice as high, the value for the tDCS with a deltoid reference might not be significant because the current density level was still far under the threshold current density used for spinal cord stimulation (23 A m^{-2}, Wesselink *et al* 1998) and to the best of our knowledge, no research has addressed any risks regarding potential spinal cord modulation by tDCS with an extracephalic reference electrode. In tDCS with an extracephalic reference under the chin or on the right buccinator muscle, no significant field concentrations in specific brain structures were observed compared to conventional tDCS results. The maximum electric field intensity and volume energy density values in the brainstem were also mildly influenced by the use of extracephalic reference electrodes.

To further evaluate the influence of the extracephalic reference electrode on tDCS current flows, we investigated the volume energy density distribution on the skin surface when the right and left deltoid references were used (figure 4). We evaluated the volume energy density (σE^2) because it is the critical parameter associated with the safety aspects due to ohmic heating. Interestingly, the energy density was concentrated at the right neck with the right deltoid reference and at the left neck with the left deltoid reference, because the dispersed currents starting from the active electrode came together while passing through the narrow portion of the neck. However, the maximum energy density amplitudes at the right and left necks were less than half of those under the electrode pads, indicating that the use of a deltoid reference electrode would not provoke any side effects on the body surface such as skin burns

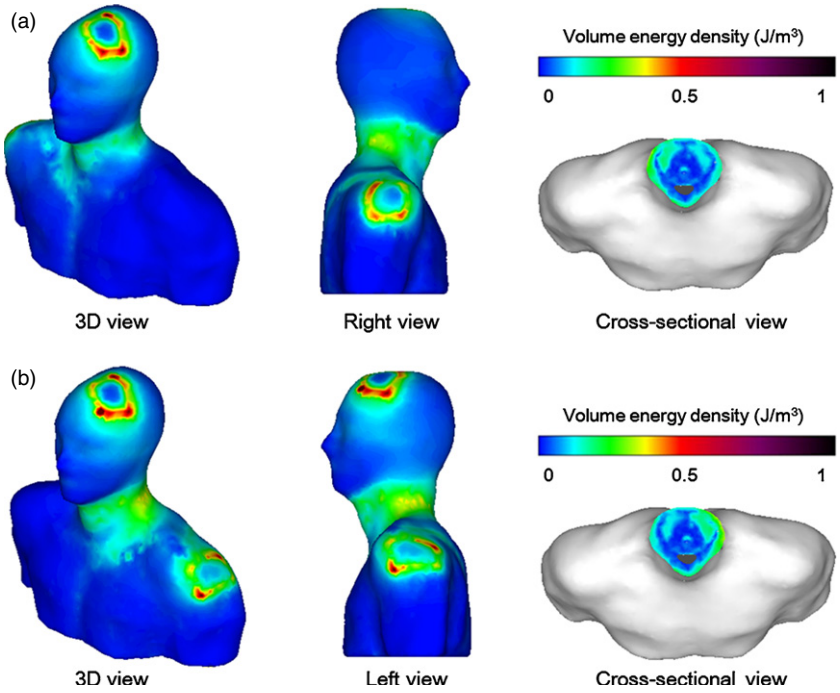

Figure 4. Volume energy density distributions on the skin surface from different viewpoints (3D view, right view, and cross-sectional view) when (a) the M1–right deltoid electrode montage and (b) the M1–left deltoid electrode montage were used.

and muscle spasms. Since no other electrode montages generated any distinct current density concentrations outside the electrode area, their distributions were not shown.

Figure 5 shows the electric field distributions on the cerebral cortex when the six different electrode montages were used. In all cases, the maximum electric fields were generated at locations slightly outside of the target area (originally under the active electrode) toward the direction of the reference electrode. This phenomenon is extensively reported in many computer simulation-based tDCS studies (Mendonca *et al* 2011, Datta *et al* 2009, Wagner *et al* 2007a). In particular, in the case of Type B (M1–contralateral supraorbital area), the generated electric field was mostly distributed around the anterior part of the brain, which was also reported in a study by Datta *et al* (figure 2.A.5 in Datta *et al* (2009)). However, it is noteworthy that the four different extracephalic reference electrode locations did not make any significant difference in the cortical field distribution due to longer current conduction paths relative to the cephalic tDCS. Our results demonstrate that the elicited cortical electric field distributions may not be significantly affected by variations in the reference electrode location in extracephalic tDCS, suggesting that the use of extracephalic reference electrodes could allow for a robust and intuitive estimation of cortical modulations even without the aid of complex field simulations.

4. Discussion

Safety is regarded as one of the key issues in the field of noninvasive brain stimulation. A number of studies have provided guidelines for the safe use of noninvasive electromagnetic

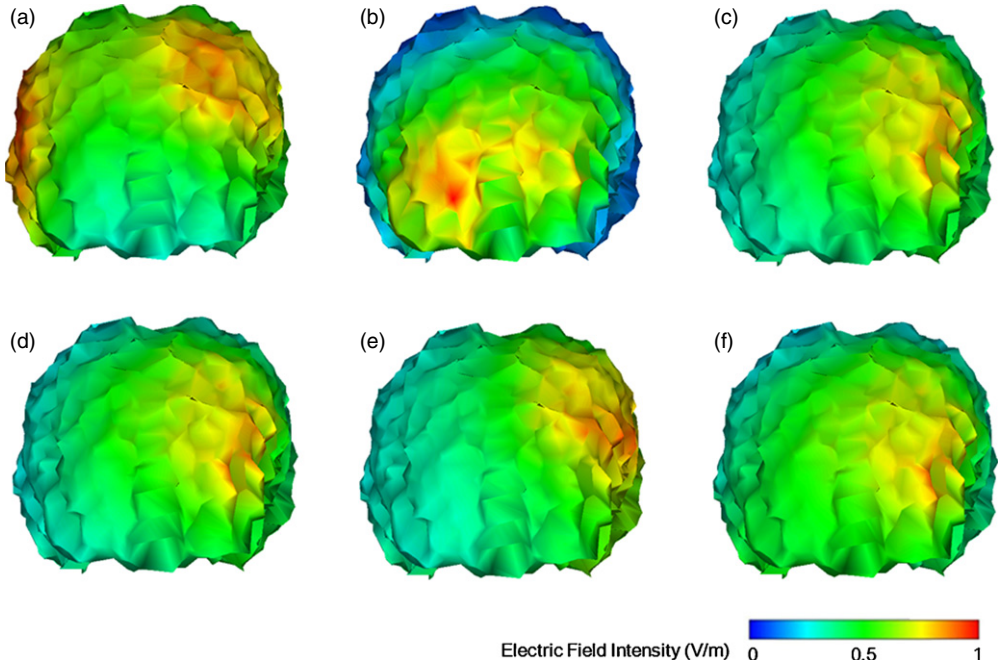

Figure 5. Electric field distributions in the cerebral cortex when six different electrode montages were used. Reference electrode locations: (a) over the right temporal lobe (Type A), (b) on the right supraorbital region (Type B), (c) on the right deltoid (Type C), (d) on the left deltoid (Type D), (e) under the chin (Type E), (f) on right buccinator muscle (Type F).

stimulation in various clinical applications and a recent review article summarized the safety guidelines in a well-organized manner (Poreisz *et al* 2007). Although the necessity of using tDCS with an extracephalic reference electrode has been raised by many researchers, whether the use of an extracephalic reference electrode could lead to an unwanted modulation of brainstem autonomic functions was still controversial. Also, though studies by Lippold and collaborators (Lippold and Redfearn 1964, Redfearn *et al* 1964) reported the possibility of the influence of an extracephalic reference electrode upon brainstem cardio-respiratory functions, a series of recent tDCS studies utilizing an extracephalic reference electrode did not report any significant changes in heart rate, blood pressure, body temperature, and respiratory frequency (Accornero *et al* 2007, Galea *et al* 2009, Koenigs *et al* 2009, Monti *et al* 2008, Vandermeeren *et al* 2010). Despite this abundant experimental evidence, no previous studies quantitatively evaluated electric fields in the brainstem generated by tDCS with an extracephalic reference electrode. To investigate the safety of extracephalic tDCS, we evaluated the current density and electric field distributions inside a simulated human upper body based on 3D FE analysis. We compared the maximum current density and electric field intensity values generated by six different electrode montages with reference electrodes over the right temporal lobe, on the right supraorbital area, on the right deltoid, on the left deltoid, under the chin, and on the right buccinator muscle, respectively. Our simulation results did not support hypotheses that the use of extracephalic reference electrodes increased electric fields in the brainstem and other sub-cortical nuclei, suggesting that the use of extracephalic reference electrodes does not lead to unwanted modulation of brainstem autonomic centers.

According to our simulation results, tDCS with an extracephalic reference electrode did not elicit more current density and electric field intensity in the brainstem than tDCS with

a cephalic reference electrode while tDCS with an extracephalic reference electrode evoked a two-fold increase in current density in the spinal cord, the location of which is not very distant from that of the brainstem, relative to the tDCS with a cephalic reference electrode. The main reason for this difference is that the brainstem is located inside the skull, which has much lower electrical conductivity than the skin. Previous simulation studies have shown that most current is conducted via the skin, and only a little penetrates through the skull for brain stimulation (Miranda *et al* 2006, Holdefer *et al* 2006, Im *et al* 2008). Our result suggests that the use of an extracephalic reference electrode does not significantly increase the amount of current penetration through the skull. Interestingly, the current density in the spinal cord was much stronger than that in the cerebral cortex in all simulations. These results indirectly support the above explanations because the spinal cord is surrounded by vertebrae that have many holes through which electric currents can flow, whereas the cerebral cortex is enclosed by the skull. We also illustrated the energy density distribution on the skin surface when the deltoid references were used (figure 4). Our simulation led to an interesting result showing concentrated energy density on the neck surface, but fortunately the maximum energy density around the neck was still lower than that around the active and reference electrode locations, demonstrating that the increased energy density around the neck would not provoke any side effects on the skin. Summarizing our simulation results, we did not detect any evidence suggesting that tDCS with an extracephalic reference electrode would be less safe than tDCS with a cephalic reference electrode.

Our FE body model had a resolution corresponding to 2.7 mm $\times$ 2.7 mm $\times$ 2.7 mm voxel size, which was relatively lower compared to a recent study (Sadleir *et al* 2010) where 1.1 mm $\times$ 1.1 mm $\times$ 1.4 mm regular voxels were used. Although our model was constructed from 1 mm $\times$ 1 mm $\times$ 1 mm resolution MRI data, it was necessary for us to find the compromise between the solution accuracy and the computational load. Considering that our model included a large portion of the body, it was difficult to use a higher resolution model for the practical field analyses. In addition, we did not consider some complex tissue structures including muscles and eyes due to the difficulty in modeling. Although the electrical conductivities of those structures were not significantly different from the surrounding tissues compared to that of fat or bone, such simplification might affect the accuracy of the field simulations to some extent, especially for the cases when extracephalic reference electrodes are attached on the facial muscles. Therefore, it will be an interesting future topic to investigate the influences of modeling accuracy, model simplification, element shapes, and model resolution on the solution accuracy of the electric field analyses. Indeed, such studies have been extensively carried out in the field of electroencephalography (EEG) source imaging (e.g. Ferguson and Stroink (1997)).

In this study, we determined electrical conductivity values for each tissue based on previously published results (Haueisen *et al* 1997, Sadleir *et al* 2010, Oostendorp *et al* 2000, Gabriel *et al* 1996a, 1996b, Holsheimer 1987). Since electric current flow is influenced by electrical conductivity values, it is obvious that an accurate estimation of tissue electrical conductivity would enhance overall accuracy of the analysis results. Indeed, some researchers even attempted to take tissue anisotropy into account for enhanced current density estimation (Suh *et al* 2009). Despite progress in medical imaging technology, the estimation of individual conductivity profiles has not yet reached to a practical level (Woo and Seo 2008). Nevertheless, considering that some EEG studies assumed large variations of individual conductivity values, up to $\pm$ 50% of the mean value (Haueisen *et al* 1997), it would be interesting to investigate the influences of individual tissue conductivity variations on the accuracy of 3D field analysis results.

Acknowledgment

This work was supported by the National Research Foundation of Korea (NRF) grant funded by the Korea government (MEST) (no 2011-0017884).

References

Accornero N, Li Voti P, La Riccia M and Gregori B 2007 Visual evoked potentials modulation during direct current cortical polarization *Exp. Brain Res.* **178** 261–6

Antal A, Kincses T Z, Nitsche M A, Bartfai O and Paulus W 2004 Excitability changes induced in the human primary visual cortex by transcranial direct current stimulation: direct electrophysiological evidence *Invest. Ophthalmol. Vis. Sci.* **45** 702–7

Antal A, Nitsche M A and Paulus W 2001 External modulation of visual perception in humans *NeuroReport* **12** 3553–5

Arfai E, Theano G, Montagu J D and Robin A A 1970 A controlled study of polarization in depression *Br. J. Psychiatry* **116** 433–4

Bernardini F, Mittleman J, Rushmeier H, Silva C and Taubin G 1999 The ball-pivoting algorithm for surface reconstruction *IEEE Trans. Vis. Comput. Graph.* **5** 349–59

Berryhill M E, Wencil E B, Coslett H B and Olson I R 2010 A selective working memory impairment after transcranial direct current stimulation to the right parietal lobe *Neurosci. Lett.* **479** 312–6

Boggio P S, Nunes A, Rigonatti S P, Nitsche M A, Pascual-Leone A and Fregni F 2007 Repeated sessions of noninvasive brain DC stimulation is associated with motor function improvement in stroke patients *Restor. Neurol. Neurosci.* **25** 123–9 PMID: 17726271

Carney M W P 1969 Brain negative polarization in the treatment of manic states *Ir. J. Med. Sci.* **2** 133–5

Christ A *et al* 2010 The Virtual Family—development of surface-based anatomical models of two adults and two children for dosimetric simulations *Phys. Med. Biol.* **55** N23–38

Cignoni P, Corsini M and Ranzuglia G 2008 Meshlab: an open-source 3D mesh processing system *ERCIM News* **73** 45–6

Cogiamanian F, Marceglia S, Ardolino G, Barbieri S and Priori A 2007 Improved isometric force endurance after transcranial direct current stimulation over the human motor cortical areas *Eur. J. Neurosci.* **26** 242–9

Datta A, Bansal V, Diaz J, Patel J, Reato D and Bikson M 2009 Gyri-precise head model of transcranial direct current stimulation: improved spatial focality using a ring electrode versus conventional rectangular pad *Brain Stimul.* **2** 201–7 PMID: 20161455

Datta A, Bikson M and Fregni F 2010 Transcranial direct current stimulation in patients with skull defects and skull plates: high-resolution computational FEM study of factors altering cortical current flow *NeuroImage* **52** 1268–78

Dmochowski J P, Datta A, Bikson M, Su Y and Parra L C 2011 Optimized multi-electrode stimulation increases focality and intensity at target *J. Neural Eng.* **8** 046011

Ferguson A S and Stroink G 1997 Factors affecting the accuracy of the boundary element method in the forward problem—I: calculating surface potentials *IEEE Trans. Biomed. Eng.* **44** 1139–55

Ferrucci R, Mameli F, Guidi I, Mrakic-Sposta S, Vergari M, Marceglia S, Cogiamanian F, Barbieri S, Scarpini E and Priori A 2008 Transcranial direct current stimulation improves recognition memory in Alzheimer disease *Neurology* **71** 493–8

Fertonani A, Rosini S, Cotelli M, Rossini P M and Miniussi C 2010 Naming facilitation induced by transcranial direct current stimulation *Behav. Brain Res.* **208** 311–8

Fregni F, Boggio P S, Nitsche M and Pascual-Leone A 2005 Transcranial direct current stimulation *Br. J. Psychiatry* **186** 446–7

Fregni F, Freedman S and Pascual-Leone A 2007 Recent advances in the treatment of chronic pain with non-invasive brain stimulation techniques *Lancet Neurol.* **6** 188–91

Fregni F and Pascual-Leone A 2007 Technology Insight: noninvasive brain stimulation in neurology-perspectives on the therapeutic potential of rTMS and tDCS *Nature Clin. Pract. Neurol.* **3** 383–93

Fregni F, Thome-Souza S, Nitsche M A, Freedman S D, Valente K D and Pascual-Leone A 2006 A controlled clinical trial of cathodal DC polarization in patients with refractory epilepsy *Epilepsia* **47** 335–42

Gabriel C, Gabriel S and Corthout E 1996a The dielectric properties of biological tissues: I. Literature survey *Phys. Med. Biol.* **41** 2231–49

Gabriel S R, Lau W and Gabriel C 1996b The dielectric properties of biological tissues: II. Measurements in the frequency range 10 Hz–20 GHz *Phys. Med. Biol.* **41** 2251–69

Galea J M, Jayaram G, Ajagbe L and Celnik P 2009 Modulation of cerebellar excitability by polarity-specific noninvasive direct current stimulation *J. Neurosci.* **29** 9115–22

Halko M A, Datta A, Plow E B, Scaturro J, Bikson M and Merabet L B 2011 Neuroplastic changes flowing rehabilitative training correlate with regional electrical field induced with tDCS *NeuroImage* **57** 885–91

Haueisen J, Ramon C, Eiselt M, Brauer H and Nowak H 1997 Influence of tissue resistivities on neuromagnetic fields and electric potentials studied with a finite element model of the head *IEEE Trans. Biomed. Eng.* **44** 727–35

Holdefer R N, Sadleir R and Russell M J 2006 Predicted current densities in the brain during transcranial electrical stimulation *Clin. Neurophysiol.* **117** 1388–97

Holsheimer J 1987 Electrical conductivity of the hippocampal CA1 layers and application to current-source-density analysis *Exp. Brain Res.* **67** 402–10

Hummel F C, Heise K, Celnik P, Floel A, Gerloff C and Cohen L G 2010 Facilitating skilled right hand motor function in older subjects by anodal polarization over the left primary motor cortex *Neurobiol. Aging* **31** 2160–8

Im C H, Jung H H, Choi J D, Jung K Y and Lee S Y 2008 Determination of optimal electrode positions for transcranial direct current stimulation (tDCS) *Phys. Med. Biol.* **53** N219–25

Jin J 2002 *The Finite Element Method in Electromagnetics* 2nd edn (New York: Wiley)

Kincses T Z, Antal A, Nitsche M A, Bartfai O and Paulus W 2004 Facilitation of probabilistic classification learning by transcranial direct current stimulation of the prefrontal cortex in the human *Neuropsychologia* **42** 113–7

Koenigs M, Ukueberuwa D, Campion P, Grafman J and Wassermann E 2009 Bilateral frontal transcranial direct current stimulation: failure to replicate classic findings in healthy subjects *Clin. Neurophysiol.* **120** 80–4

Lippold O C and Redfearn J W 1964 Mental changes resulting from the passage of small direct currents through the human brain *Br. J. Psychiatry* **110** 768–72

Mahmoud H, Haghighi A B, Petramfar P, Jahanshahi S, Salehi Z and Fregni F 2010 Transcranial direct current stimulation: electrode montage in stroke *Disabil. Rehabil.* **33** 1383–8

Mendonca M E, Santana M B, Baptista A F, Datta A, Bikson M, Fregni F and Araujo C P 2011 Transcranial DC stimulation in fibromyalgia: optimized cortical target supported by high-resolution computational models *J. Pain* **12** 610–7

Mignon A, Laudenbach V, Guischard F, Limoge A, Desmonts J M and Mantz J 1996 Transcutaneous cranial electrical stimulation (Limoge's currents) decreases early buprenorphine analgesic requirements after abdominal surgery *Anesth. Analg.* **83** 771–5 PMID: 8831319

Miranda P C, Correia L, Salvador R and Basser P J 2007 Tissue heterogeneity as a mechanism for localized neural stimulation by applied electric fields *Phys. Med. Biol.* **52** 5603–17

Miranda P C, Lomarev M and Hallett M 2006 Modeling the current distribution during transcranial direct current stimulation *Clin. Neurophysiol.* **117** 1623–9

Moliadze V, Antal A and Paulus W 2010 Electrode-distance dependent after-effects of transcranial direct and random noise stimulation with extracephalic reference electrodes *Clin. Neurophysiol.* **121** 2165–71

Monti A, Cogiamanian F, Marceglia S, Ferrucci R, Mameli F, Mrakic-Sposta S, Vergari M, Zago S and Priori A 2008 Improved naming after transcranial direct current stimulation in aphasia *J. Neurol. Neurosurg. Psychiatry* **79** 451–3

Nitsche M A, Boggio P S, Fregni F and Pascual-Leone A 2009 Treatment of depression with transcranial direct current stimulation (tDCS): a review *Exp. Neurol.* **219** 14–9

Nitsche M A, Doemkes S, Karakose T, Antal A, Liebetanz D, Lang N, Tergau F and Paulus W 2007 Shaping the effects of transcranial direct current stimulation of the human motor cortex *J. Neurophysiol.* **97** 3109–17

Nitsche M A *et al* 2008 Transcranial direct current stimulation: state of the art *Brain Stimul.* **1** 206–23

Nitsche M A and Paulus W 2000 Excitability changes induced in the human motor cortex by weak transcranial direct current stimulation *J. Physiol.* **527** 633–9

Oostendorp T F, Delbeke J and Stegeman D F 2000 The conductivity of the human skull: results of *in vivo* and *in vitro* measurements *IEEE Trans. Biomed. Eng.* **47** 1487–92

Park J H, Hong S B, Kim D W, Suh M and Im C H 2011 A novel array-type transcranial direct current stimulation (tDCS) system for accurate focusing on targeted brain areas *IEEE Trans. Magn.* **47** 882–5

Poreisz C, Boros K, Antal A and Paulus W 2007 Safety aspects of transcranial direct current stimulation concerning healthy subjects and patients *Brain Res. Bull.* **72** 208–14

Priori A 2003 Brain polarization in humans: a reappraisal of an old tool for prolonged non-invasive modulation of brain excitability *Clin. Neurophysiol.* **114** 589–95

Priori A, Berardelli A, Rona S, Accornero N and Manfredi M 1998 Polarization of the human motor cortex through the scalp *NeuroReport* **9** 2257–60

Priori A, Mameli F, Cogiamanian F, Marceglia S, Tiriticco M, Mrakic-Sposta S, Ferrucci R, Zago S, Polezzi D and Sartori G 2008 Lie-specific involvement of dorsolateral prefrontal cortex in deception *Cereb. Cortex* **18** 451–5

Redfearn J W, Lippold O C and Costain R 1964 A preliminary account of the clinical effects of polarizing the brain in certain psychiatric disorders *Br. J. Psychiatry* **110** 773–85

Sadleir R J, Vannorsdall T D, Schretlen D J and Gordon B 2010 Transcranial direct current stimulation (tDCS) in a realistic head model *NeuroImage* **51** 1310–8

Schlaug G, Renga V and Nair D 2008 Transcranial direct current stimulation in stroke recovery *Arch. Neurol.* **65** 1571–6

Si H 2008 Adaptive tetrahedral mesh generation by constrained Delaunay refinement *Int. J. Numer. Methods Eng.* **75** 856–80

Suh H S, Kim S H, Lee W H and Kim T S 2009 Realistic simulation of transcranial direct current stimulation via 3-D high-resolution finite element analysis: effect of tissue anisotropy *Proc. IEEE Ann. Int. Conf. EMBC* pp 638–41

Vandermeeren Y, Jamart J and Ossemann M 2010 Effect of tDCS with an extracephalic reference electrode on cardio-respiratory and autonomic functions *BMC Neurosci.* **11** 38

Vollmer F, Mencl R and Müller H 1999 Improved Laplacian smoothing of noisy surface meshes *Comput. Graph. Forum* **18** 131–8

Wagner T, Fregni F, Fecteau S, Grodzinsky A, Zahn M and Pascual-Leone A 2007a Transcranial direct current stimulation: a computer-based human model study *NeuroImage* **35** 1113–24

Wagner T, Valero-Cabre A and Pascual-Leone A 2007b Noninvasive human brain stimulation *Ann. Rev. Biomed. Eng.* **9** 527–65

Wesselink W A, Holsheimer J and Boom H B K 1998 Analysis of current density and related parameters in spinal cord stimulation *IEEE Trans. Rehabil. Eng.* **6** 200–7

Williams J A, Imamura M and Fregni F 2009 Updates on the use of non-invasive brain stimulation in physical and rehabilitation medicine *J. Rehabil. Med.* **41** 305–11

Woo E J and Seo J K 2008 Magnetic resonance electrical impedance tomography (MREIT) for high-resolution conductivity imaging *Physiol. Meas.* **29** R1–26